Fourier-transform quantum state tomography

Mohammadreza Mohammadi, Agata M. Brańczyk,[*] and Daniel F. V. James

CQIQC and IOS, Department of Physics, University of Toronto, 60 Saint George Street, Toronto, Ontario M5S 1A7, Canada

(Received 14 November 2012; published 17 January 2013)

We propose a technique for performing quantum state tomography of photonic polarization-encoded multiqubit states. Our method uses a single *rotating* wave plate, a polarizing beam splitter, and two photon-counting detectors per photon mode. As the wave plate rotates, the photon counters measure a pseudocontinuous signal which is then Fourier transformed. The density matrix of the state is reconstructed using the relationship between the Fourier coefficients of the signal and the Stokes' parameters that represent the state. The experimental complexity, i.e., different wave plate rotation frequencies, scales linearly with the number of qubits.

Quantum state preparation is an essential ingredient in the realization of quantum technologies such as quantum computing [1], quantum cryptography [2], and other quantum information protocols [3]. A crucial aspect of reliable state preparation is the ability to accurately characterize the state of a quantum system. To this end, quantum state tomography (QST) allows the reconstruction of a state's density matrix from measurement statistics accumulated through repeated independent measurements of multiple identically prepared systems [4–6].

In linear optics, where quantum information is encoded in the polarization of a single photon, different measurement settings are realized with a combination of linear optical elements such as wave plates, beam splitters, and polarizing beam splitters, followed by photon counting. QST was first accomplished in such systems by White *et al.* [7], where the measurement settings corresponded directly to the Stokes' parameters used to characterize the polarization state of the classical electromagnetic field [8]. Later it was suggested that an over-complete symmetric six-measurement set [9] or an informationally complete symmetric four-measurement set [9–13] be used for improved performance. Other extensions, such as those considering optimal experimental design under realistic technical constraints [14,15], or modifications due to inaccessible information [16–22] or preferable measurement choices [9,11,12,23–30] have also been considered.

To date, implementations of QST of photonic polarization-encoded qubits have utilized either multiple wave plates and/or multiple beam splitters per qubit. We propose a technique that uses only one wave plate and one polarizing beam splitter (PBS) per qubit mode. Each mode m is incident on a single wave plate rotating at frequency Ω_m followed by a polarizing beam splitter (PBS). Photon counters at the output ports of the PBS measure a pseudocontinuous signal and the state is reconstructed from the Fourier coefficients of this signal. The experimental complexity of this method scales linearly with the number of qubits in terms of the number of settings required (i.e., wave-plate rotation frequencies) rather than exponentially, as is the case with QST that uses discrete measurement settings. Similar techniques that rely on rotating wave plates are used in classical optics to determine the

polarization state of the electromagnetic field [31]. In the context of nonclassical light, Fourier spectroscopy has been used to characterize the joint spectrum of photons [32].

The remainder of this paper is organized as follows. In Sec. I, we give a brief review of QST of multiqubit states. In Sec. II, we introduce our scheme for Fourier transform tomography (FTT) and provide examples for one and two qubits. In Sec. III, we provide concluding remarks.

I. QUANTUM STATE TOMOGRAPHY

Tomography is the process of constructing a representation of an object by imaging it in different sections. In quantum state tomography, we aim to construct a representation of a quantum state $\hat{\rho}$ from different measurement outcomes. An n-qubit system is specified by $4^n - 1$ real parameters. We therefore require at least this many outcomes of linearly independent measurements to specify $\hat{\rho}$.

The probability of obtaining measurement outcome j, given a measurement operator $\hat{M}_j$, is given by

$$p_j = \langle \hat{M}_j \rangle = \mathrm{Tr}[\hat{\rho}\hat{M}_j] = \frac{n_j}{\mathcal{N}_j}, \qquad (1)$$

where n_j is the number of counts and $\mathcal{N}_j$ is a constant dependent on the detector efficiency and duration of data collection. In a polarization-encoded linear optical system, any projective measurement can be realized with a quarter-wave plate, a half-wave plate, and a polarizing beam splitter, as shown in Fig. 1(a). A popular choice corresponds to the three Pauli operators.

We can always write the density matrix of an n-qubit system in terms of Hermitian operators $\hat{\sigma}_i$,

$$\hat{\rho} = \frac{1}{2^n} \sum_{i_1,\dots,i_n=0}^{3} S_{i_1,\dots,i_n} \hat{\sigma}_{i_1} \otimes \cdots \otimes \hat{\sigma}_{i_n}, \qquad (2)$$

where $\hat{\sigma}_0 = |H\rangle\langle H| + |V\rangle\langle V|$ is the identity operator and $\hat{\sigma}_{1-3}$ are the Pauli operators: $\hat{\sigma}_1 = |H\rangle\langle V| + |V\rangle\langle H|$, $\hat{\sigma}_2 = i(|V\rangle\langle H| - |H\rangle\langle V|)$, and $\hat{\sigma}_3 = |H\rangle\langle H| - |V\rangle\langle V|$. The coefficients $S_{i_1,\dots,i_n} = \mathrm{Tr}[\hat{\rho}(\hat{\sigma}_{i_1} \otimes \cdots \otimes \hat{\sigma}_{i_n})]$ completely characterize the state. $S_{i_1,\dots,i_n}$ are normalized generalizations of the classical parameters introduced by Stokes in 1852 [8], and will hereafter be simply referred to as *Stokes' parameters*.

_____
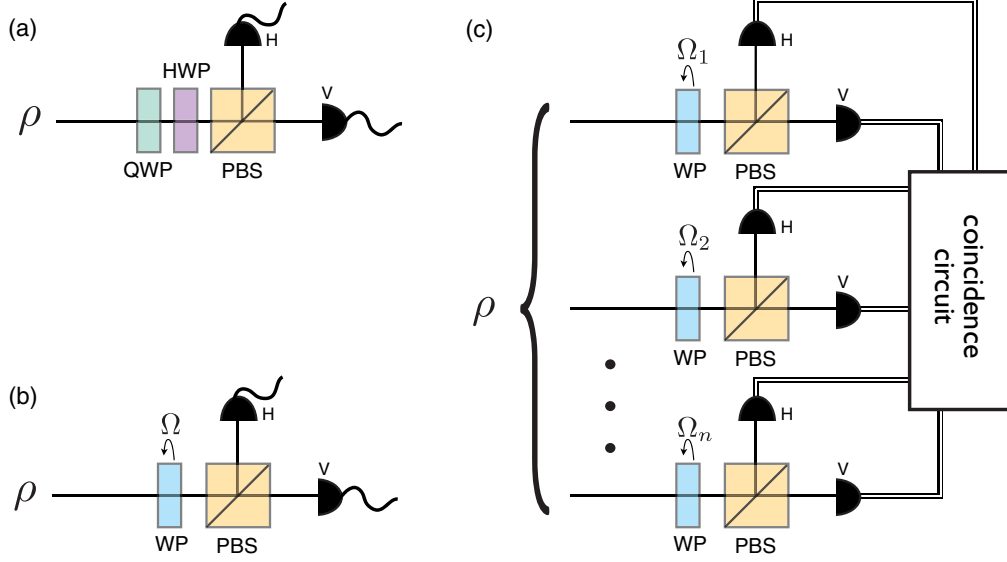*branczyk@physics.utoronto.ca

FIG. 1. (Color online) Schematic diagrams of (a) typical QST setup which uses a combination of quarter- and half-wave plates to perform arbitrary-basis measurements; (b) FTT setup which uses one rotating wave plate; (c) multiqubit FTT which uses one wave plate per qubit mode m, rotating at frequency Ω_m.

Combining Eqs. (1) and (2), we find a linear relationship between Stokes' parameters and the probability p_j:

$$p_j = \frac{1}{2^n} \sum_{i_1,\dots,i_n=0}^{3} S_{i_1,\dots,i_n} \text{Tr}\big[\hat{\sigma}_{i_1} \otimes \cdots \otimes \hat{\sigma}_{i_n} \hat{M}_j\big], \qquad (3)$$

where $\hat{M}_j$ acts on the entire multiqubit system. By making $4^n - 1$ linearly independent measurements, it is possible to solve for Stokes' parameters and reconstruct the density matrix according to Eq. (2). This can be achieved through a variety of methods, including simple linear inversion, least-squares estimation or the popular maximum likelihood estimation method [33]. Alternatively, one can look to a growing number of exciting new techniques such as the forced purity routine [34], Baysean mean estimation [35], compressed sensing [36], von Neumann entropy maximization [37], hedged maximum likelihood estimation [38], minimax estimation [39], and techniques that focus on reconstructing the state with reliable error bars [40] and confidence regions [41].

II. FOURIER TRANSFORM TOMOGRAPHY

In this section, we show how the quantum state of a multiqubit system can be represented by a single joint-probability signal and how the measurement of this signal enables the reconstruction of the quantum state.

In our proposal, identical copies of the state are prepared and subsequently pass through a series of optical elements. For a multiphoton state, each photon mode m is incident on a single wave plate rotating at frequency Ω_m followed by a polarizing beam splitter (PBS). Photon counters at the output ports of the PBS continuously measure the intensity, which can be processed to recover Stokes' parameters. A schematic of this setup is shown in in Fig. 1(b) for a single qubit and Fig. 1(c) for multiple qubits. For multiple qubits, the signal

measured is a "coincidence intensity" corresponding to the joint probability of detecting photons at each PBS.

The time-dependent single-qubit projection-valued measure (PVM) associated with the probability of detecting a photon in the horizontal or vertical output modes of each PBS is given by $\{\hat{M}_m^H(t), \hat{M}_m^V(t)\}$ where

$$\hat{M}_m^a(t) = \hat{U}_m^\dagger |a\rangle\langle a| \hat{U}_m, \qquad (4)$$

for $a = H, V$, where m labels the qubit mode and

$$\hat{U}_m(t) = \cos\left(\frac{\beta}{2}\right)\hat{\sigma}_0 - i\sin\left(\frac{\beta}{2}\right)\vec{v}_m(t)\cdot\vec{\sigma} \qquad (5)$$

is the unitary operator associated with a wave plate in mode m. $\hat{U}_m(t)$ rotates the operators $|a\rangle\langle a|$ on the Bloch sphere by an angle β, about the vector,

$$\vec{v}_m(t) = \cos(\omega_m t)\vec{k} + \sin(\omega_m t)\vec{i}, \qquad (6)$$

where $\vec{k}$ and $\vec{i}$ are unit vectors in Euclidian space (defined by the axes in Fig. 2) and $\vec{v}\cdot\vec{\sigma} = v_1\hat{\sigma}_1 + v_2\hat{\sigma}_2 + v_3\hat{\sigma}_3$. As the wave plate rotates about the beam axis at frequency Ω_m in real space, $\vec{v}_m(t)$ rotates about the y axis in Euclidian space at frequency $\omega_m = 2\Omega_m$. We assume that the fast axis of the wave plate is aligned at 0 degrees to the horizontal as defined by the polarization of the photons. A phase factor can be included in $\vec{v}_m(t)$ to account for different initial alignment of the wave plate. The resulting projector $\hat{M}_m^H(t)$ traces out a figure-eight path on the Bloch sphere, as shown in Fig. 2. The retardance of the wave plate β determines the size of the figure eight.

To characterize an n-qubit state, one measures a joint probability of detecting a photon in the H mode of each PBS. This is given by

$$p_n(t) = \frac{1}{2^n} \sum_{i_1,\dots,i_n=0}^{3} S_{i_1\dots,i_n} \chi_{1,i_1} \cdots \chi_{n,i_n}, \qquad (7)$$
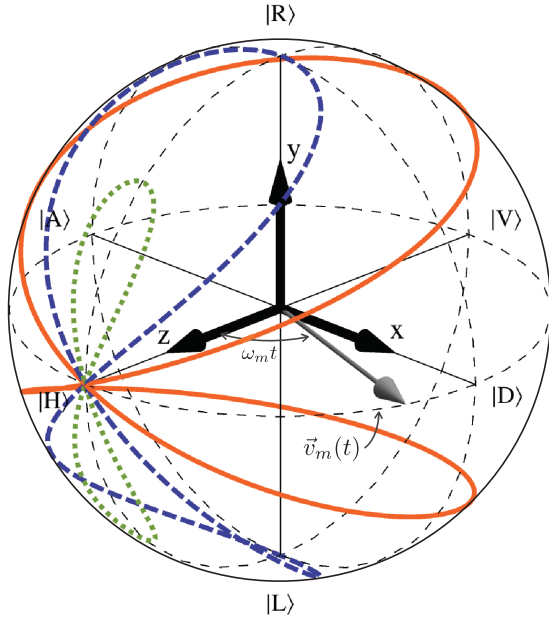
FIG. 2. (Color online) Path traced out by $\hat{M}_m^{(H)}(t)$, defined in Eq. (4), for $\beta = \pi/4$ (green, dotted); $\beta = \pi/2$ (blue, dashed); and $\beta = 11\pi/15$ (orange, solid).

where

$$\chi_{m,i} := \text{Tr}\left[\hat{\sigma}_i \hat{M}_m^H(t)\right], \tag{8}$$

and therefore

$$\chi_{m,0} = 1, \tag{9a}$$
$$\chi_{m,1} = s^2 \sin(2\omega_m t), \tag{9b}$$
$$\chi_{m,2} = 2cs \sin(\omega_m t), \tag{9c}$$
$$\chi_{m,3} = c^2 + s^2 \cos(2\omega_m t), \tag{9d}$$

where $c = \cos(\beta/2)$ and $s = \sin(\beta/2)$.

Note that the choice of analyzing the signal from mode H rather than mode V is arbitrary and typically both modes will need to be measured to ensure normalized probabilities.

Without loss of generality, we restrict $0 < \omega_1 < \ldots < \omega_n$. For two qubits, $\omega_2 = r\omega_1$ where $r > 1$. If r is an irrational number, the signal does not have a finite period. If r is a rational number, we can write $r = p/q$, where p and q are integers. In this case, the period of the two-qubit signal is given by

$$T(r) = \frac{2\pi q}{\omega_1 \gcd(p,q)}, \tag{10}$$

where $\gcd(p,q)$ is the greatest common denominator of p and q. For $n > 2$, the period of the signal can be determined via recursion. A shorter period is favorable from an experimental perspective which, for a constant ω_1, occurs when r is an integer. The lowest integer that ensures sufficient Fourier coefficients to solve for Stokes' parameters is $r = 5$.

In practice p_n will not be a continuous function of time but rather a discretized approximation. The discretized signal will be divided into time bins, with $\mathcal{N}$ coincidence counts in each bin. The number of time bins per period, N, must be at least the Nyquist rate, i.e. twice the highest frequency contained within the signal, to avoid aliasing.
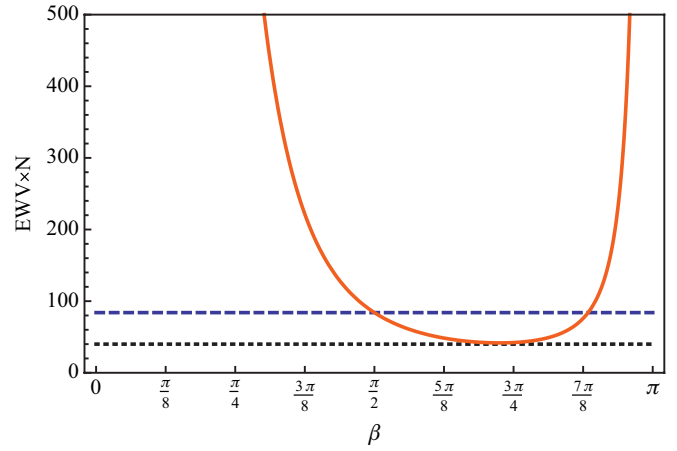

FIG. 3. (Color online) The equally weighted variance (EWV) [42] assesses the noise immunity of the wave plate. Here we plot EWV $\times$ N for one period as a function of β (orange, solid), where N is the total number of bins per period. A smaller EWV is associated with better immunity to noise. The best noise immunity occurs at $\beta \approx 2.27 \approx 11\pi/15$ for EWV $\approx 41.7/N$. The black, dotted line shows EWV$^{\text{opt}} = 40/N$, attainable by optimal tomographic schemes such as those that measure the Pauli matrices or the SIC-POVM [10,11,13]. The blue, dashed line shows the EWV for a QWP ($\beta = \pi/2$), EWV$^{\text{QWP}} = 84/N$. Note that the EWV is dimensionless.

The discrete probability in bin τ_j will be given by

$$p_n(\tau_j) = \frac{n_{H\ldots H}}{\mathcal{N}}, \tag{11}$$

where $\mathcal{N} = \sum_{k_1,\ldots,k_{2^n}=H,V} n_{k_1,\ldots,k_{2^n}}$, n is the number of qubits and $n_{k_1,\ldots,k_{2^n}}$ is the number of coincidence counts for a given projector $\hat{M}_m^{k_1}(t) \otimes \cdots \otimes \hat{M}_m^{k_{2^n}}(t)$.

In principle, β can take on any value other than an integer multiple of π. However, in practice, some values will be more susceptible to noise than others. We use the equally weighted variance (EWV) [42], which assesses the noise immunity of the wave plate, to show that $\beta \approx 11\pi/15$ is most immune to noise, as defined in Ref. [42]. A plot of the EWV is shown in Fig. 3. Such a retardance can be achieved with an off-the-shelf wave plate designed for a wave length different to that of the experiment.

In the remainder of this section, we provide specific examples for one- and two-qubit states.

A. Example: one qubit

For a single qubit, the signal is given by

$$p_1(t) = \frac{1}{2} \sum_{i=0}^{3} S_i \chi_{1,i} \tag{12a}$$

$$= \frac{S_0}{2} + \frac{S_1}{2} s^2 \sin(2\omega_1 t) + S_2 cs \sin(\omega_1 t)$$
$$+ \frac{S_3}{2} [c^2 + s^2 \cos(2\omega_1 t)]. \tag{12b}$$

This can be written as

$$p_1(t) \equiv \frac{a_0}{2} + b_1 \sin(\omega_1 t) + a_2 \cos(2\omega_1 t) + b_2 \sin(2\omega_1 t), \tag{13}$$
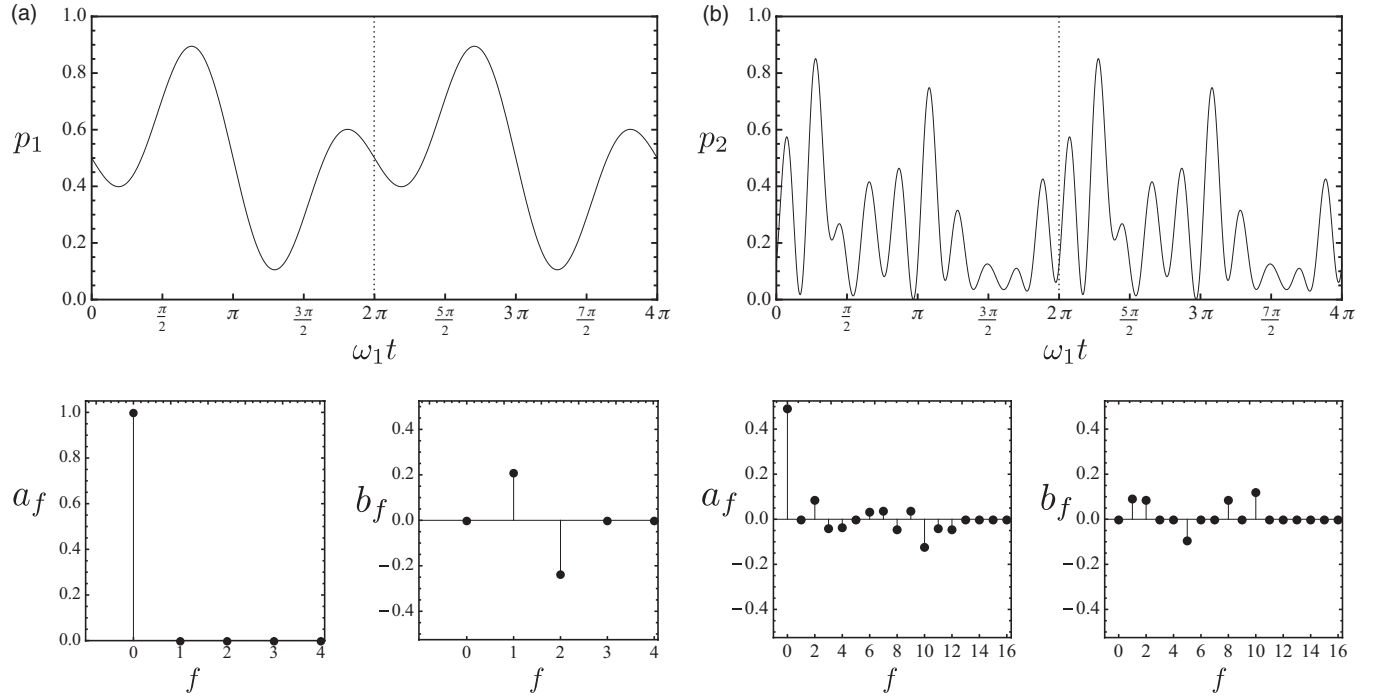
FIG. 4. The probability signal p_n, as a function of revolutions of the first wave plate, and Fourier coefficients a_f and b_f for the state: (a) $\hat{\rho}_1$ given in Eq. (17); and (b) $|\psi\rangle_2$ given in Eq. (21). The label f denotes the term in the Fourier series and corresponds to the subscript in Eqs. (13) and (20b).

where the Fourier coefficients are given by

$$a_0 = S_0 + S_3 c^2; \tag{14a}$$

$$b_1 = S_2 cs; \tag{14b}$$

$$a_2 = \frac{S_3}{2} s^2; \tag{14c}$$

$$b_2 = \frac{S_1}{2} s^2, \tag{14d}$$

where $c = \cos(\beta/2)$ and $s = \sin(\beta/2)$. Linear inversion of Eq. (14) gives the Stokes' parameters in terms of the Fourier coefficients:

$$S_0 = a_0 - \frac{2a_2 c^2}{s^2}; \tag{15a}$$

$$S_1 = \frac{2b_2}{s^2}; \tag{15b}$$

$$S_2 = \frac{b_1}{cs}; \tag{15c}$$

$$S_3 = \frac{2a_2}{s^2}. \tag{15d}$$

Substitution into Eq. (2), gives the density matrix in terms of the Fourier coefficients:

$$\rho_1 = \begin{pmatrix} \frac{1}{2}(a_0 + 2a_2) & \frac{b_2}{s^2} - i\frac{b_1}{2cs} \\ \frac{b_2}{s^2} + i\frac{b_1}{2cs} & \frac{1}{2}(a_0 + 2a_2) - \frac{2a_2}{s^2} \end{pmatrix}. \tag{16}$$

As an example, consider a single-qubit state $|\psi\rangle_1$ that has experienced depolarizing noise, characterized by the parameter d, such that

$$\hat{\rho}_1 = d|\psi\rangle_1\langle\psi|_1 + (1-d)\hat{\sigma}_z|\psi\rangle_1\langle\psi|_1\hat{\sigma}_z. \tag{17}$$

Specifically, let's consider

$$|\psi\rangle_1 = \frac{1}{\sqrt{2}}(|H\rangle + e^{-i\pi/4}|V\rangle), \tag{18}$$

and $d = 0.1$. A retardance of $\beta = 11\pi/15$ produces the signal shown in Fig. 4(a). Performing a fast Fourier transform (FFT) of the discretized signal yields the Fourier coefficients in Fig. 4(a). The coefficients a_f and b_f correspond to the real and imaginary parts of the list generated by the FFT, respectively. Inserting the coefficients, $a_0 = 1$, $b_1 = 0.210$, $a_2 = 0$, and $b_2 = -0.236$ into the density matrix in Eq. (16) gives

$$\rho_1 = \begin{pmatrix} 0.5 & -0.283 - 0.283i \\ -0.283 + 0.283i & 0.5 \end{pmatrix}, \tag{19}$$

which corresponds to the density operator in Eq. (17) for $d = 0.1$.

B. Example: two qubits

For two qubits, the joint probability of detecting a photon in the horizontal output ports of each PBS is given by

$$p_2(t) = \sum_{i_1,i_2=0}^{3} \frac{S_{i_1,i_2}}{4} \chi_{1,i_1} \chi_{2,i_2} \tag{20a}$$

$$= \frac{a_0}{2} + \sum_{f=1}(a_f \cos(\omega'_f t) + b_f \sin(\omega'_f t)), \tag{20b}$$

where in the second line, we have written the signal in terms of its Fourier coefficients. The extent of the summation depends on the specific choice of relative frequencies, and ω'_f are

functions of ω_1 and ω_2 from the set $\{\omega_1, \omega_2, 2\omega_1, 2\omega_2, \omega_1 \pm \omega_2, \omega_1 \pm 2\omega_2, 2\omega_1 \pm \omega_2, 2\omega_1 \pm 2\omega_2\}$. The elements of this set are not necessarily in order of size, and to relate them to ω_f' one needs to consider explicit values for ω_1 and ω_2.

As an example, consider the two-qubit state,

$$|\psi\rangle_2 = \frac{1}{\sqrt{2}} (|H\rangle|V\rangle + |R\rangle|L\rangle). \qquad (21)$$

Wave-plate retardances of $\beta = 11\pi/15$ and a frequency ratio $r = \omega_2/\omega_1 = 5$ produces the signal shown in Fig. 4(b). The

explicit expression for $p_2(t)$ for this choice of measurement settings can be found in Eq. (A2). Performing a fast Fourier transform (FFT) of the discretized signal yields the Fourier coefficients in Fig. 4(b).

Linear inversion of the expressions for the Fourier coefficients in terms of the Stokes' parameters, given in Eq. (A3), followed by substitution into Eq. (2), along with the Fourier coefficients determined from the signal in Fig. 4(b), gives the reconstructed density matrix,

$$\rho_2 = \begin{pmatrix} 0.125 & 0.25 + 0.125i & -0.125i & 0.125 \\ 0.25 - 0.125i & 0.625 & -0.125 - 0.25i & 0.25 - 0.125i \\ 0.125i & -0.125 + 0.25i & 0.125 & 0.125i \\ 0.125 & 0.25 + 0.125i & -0.125i & 0.125 \end{pmatrix}, \qquad (22)$$

which corresponds to the density operator $\hat{\rho}_2 = |\psi\rangle_2\langle\psi|_2$ where $|\psi\rangle_2$ is defined in Eq. (21). In general, given separable qubits, p_2 factorizes into a product of p_1 for each qubit.

III. SUMMARY & CONCLUDING REMARKS

We presented a scheme for performing quantum state tomography of photonic polarization-encoded multiqubit states. The scheme is simpler than standard tomographic protocols in that only one wave plate and one polarizing beam splitter is required per photon mode.

In this scheme, photon-counting detectors measure a pseudocontinuous time-dependent joint probability as the wave plates rotate at frequency Ω_m. The Fourier coefficients of the signal give the Stokes' parameters which describe the state. For a single qubit, the optimal wave-plate retardance is $\beta \approx 11\pi/15$.

This technique reduces the number of required optical elements and the experimental complexity scales linearly with the number of qubits, in terms of the number of settings required (wave-plate rotation frequencies) rather than exponentially, as is the case with QST that uses discrete measurement settings.

An open question is whether the representation of a quantum state as a continuous signal will provide intuitive means for establishing certain properties of the state such as its entanglement.

APPENDIX: PROBABILITY SIGNAL AND FOURIER COEFFICIENTS FOR TWO-QUBIT STATE

In this Appendix, we give the probability signal for the specific two-qubit example described in Sec. II B. We also

provide expressions for the Fourier coefficients in terms of the Stokes' parameters, as well as the inverted expressions for the Stokes' parameters in terms of the Fourier coefficients.

The signal probability for the state,

$$|\psi\rangle_2 = \frac{1}{\sqrt{2}} (|H\rangle|V\rangle + |R\rangle|L\rangle), \qquad (A1)$$

with a frequency ratio $r = \omega_2/\omega_1 = 5$, is

$$\begin{aligned} p_2(t) = \frac{a_0}{2} &+ b_1 \sin(\omega_1 t) + b_2 \sin(2\omega_1 t) + b_3 \sin(3\omega_1 t) \\ &+ b_5 \sin(5\omega_1 t) + b_7 \sin(7\omega_1 t) + b_8 \sin(8\omega_1 t) \\ &+ b_9 \sin(9\omega_1 t) + b_{10} \sin(10\omega_1 t) + b_{11} \sin(11\omega_1 t) \\ &+ b_{12} \sin(12\omega_1 t) + a_2 \cos(2\omega_1 t) + a_3 \cos(3\omega_1 t) \\ &+ a_8 \cos(8\omega_1 t) + a_4 \cos(4\omega_1 t) + a_6 \cos(6\omega_1 t) \\ &+ a_7 \cos(7\omega_1 t) + a_9 \cos(9\omega_1 t) + a_{10} \cos(10\omega_1 t) \\ &+ a_{11} \cos(11\omega_1 t) + a_{12} \cos(12\omega_1 t), \qquad (A2) \end{aligned}$$

where the Fourier coefficients are

$$a_0 = (c^2(c^2 S_{3,3} + S_{0,3} + S_{3,0}) + S_{0,0})/2, \qquad (A3a)$$
$$a_2 = s^2(c^2 S_{3,3} + S_{3,0})/4, \qquad (A3b)$$
$$a_3 = -a_7 = cs^3 S_{1,2}/4, \qquad (A3c)$$
$$a_4 = -a_6 = c^2 s^2 S_{2,2}/2, \qquad (A3d)$$
$$a_8 = s^4(S_{1,1} + S_{3,3})/8, \qquad (A3e)$$
$$a_9 = -a_{11} = cs^3 S_{2,1}/4, \qquad (A3f)$$
$$a_{10} = s^2(c^2 S_{3,3} + S_{0,3})/4, \qquad (A3g)$$
$$a_{12} = s^4(S_{3,3} - S_{1,1})/8, \qquad (A3h)$$

and

$$b_1 = cs(c^2 S_{2,3} + S_{2,0})/2, \qquad (A4a)$$
$$b_2 = s^2(c^2 S_{1,3} + S_{1,0})/2, \qquad (A4b)$$
$$b_3 = b_7 = cs^3 S_{3,2}/4, \qquad (A4c)$$
$$b_5 = cs(c^2 S_{3,2} + S_{0,2})/2, \qquad (A4d)$$
$$b_8 = s^4(S_{3,1} - S_{1,3})/8, \qquad (A4e)$$

$$b_9 = -b_{11} = -cs^3 S_{2,3}/4, \tag{A4f}$$

$$b_{10} = s^2(c^2 S_{3,1} + S_{0,1})/4, \tag{A4g}$$

$$b_{12} = s^4(S_{1,3} + S_{3,1})/8, \tag{A4h}$$

where $c = \cos(\beta/2)$ and $s = \sin(\beta/2)$. Inverting Eqs. (A3) and (A4) gives

$$S_{0,0} = 4c^2((a_8 + a_{12})c^2 - (a_2 + a_{10})s^2)/s^4 + 2a_0, \tag{A5a}$$

$$S_{0,1} = -4((b_8 + b_{12})c^2 - b_{10}s^2)/s^4, \tag{A5b}$$

$$S_{0,2} = 2b_5/cs - 4b_3c/s^3, \tag{A5c}$$

$$S_{0,3} = 4a_{10}/s^2 - 4(a_8 + a_{12})c^2/s^4, \tag{A5d}$$

$$S_{1,0} = 4((b_8 - b_{12})c^2 + b_2s^2)/s^4, \tag{A5e}$$

$$S_{1,1} = 4(a_8 - a_{12})/s^4, \tag{A5f}$$

$$S_{1,2} = 4a_3/cs^3, \tag{A5g}$$

$$S_{1,3} = -4(b_8 - b_{12})/s^4, \tag{A5h}$$

$$S_{2,0} = 4b_9c/s^3 + 2b_1/cs, \tag{A5i}$$

$$S_{2,1} = 4a_9/cs^3, \tag{A5j}$$

$$S_{2,2} = 2a_4/c^2s^2, \tag{A5k}$$

$$S_{2,3} = -4b_9/cs^3, \tag{A5l}$$

$$S_{3,0} = 4a_2/s^2 - 4(a_8 + a_{12})c^2/s^4, \tag{A5m}$$

$$S_{3,1} = 4(b_8 + b_{12})/s^4, \tag{A5n}$$

$$S_{3,2} = 4b_3/cs^3, \tag{A5o}$$

$$S_{3,3} = 4(a_8 + a_{12})/s^4. \tag{A5p}$$

Substituting the Stokes' parameters, along with the Fourier coefficients in Fig. 4(b), into Eq. (2), gives the reconstructed density matrix in Eq. (22) which corresponds to the density operator $\hat{\rho}_2 = |\psi\rangle_2\langle\psi|_2$ where $|\psi\rangle_2$ is defined in Eq. (A1).

[1] P. Kok and B. W. Lovett, *Introduction to Optical Quantum Information Processing*, 1st ed. (Cambridge University Press, Cambridge, 2010).

[2] C. H. Bennett and G. Brassard, in *Proceedings of IEEE International Conference on Computers, Systems and Signal Processing* (IEEE, New York, 1984), pp. 175–179.

[3] M. A. Nielsen and I. L. Chuang, *Quantum Computation and Quantum Information* (Cambridge University Press, Cambridge, 2000).

[4] K. Vogel and H. Risken, Phys. Rev. A **40**, 2847 (1989).

[5] U. Leonhardt, Phys. Rev. Lett. **74**, 4101 (1995).

[6] D. F. V. James, P. G. Kwiat, W. J. Munro, and A. G. White, Phys. Rev. A **64**, 052312 (2001).

[7] A. G. White, D. F. V. James, P. H. Eberhard, and P. G. Kwiat, Phys. Rev. Lett. **83**, 3103 (1999).

[8] G. C. Stokes, Cambridge Philos. Soc **9**, 399 (1852).

[9] M. D. de Burgh, N. K. Langford, A. C. Doherty, and A. Gilchrist, Phys. Rev. A **78**, 052122 (2008).

[10] J. Řeháček, B.-G. Englert, and D. Kaszlikowski, Phys. Rev. A **70**, 052321 (2004).

[11] A. Ling, K. P. Soh, A. Lamas-Linares, and C. Kurtsiefer, Phys. Rev. A **74**, 022309 (2006).

[12] Z. E. D. Medendorp, F. A. Torres-Ruiz, L. K. Shalm, G. N. M. Tabia, C. A. Fuchs, and A. M. Steinberg, Phys. Rev. A **83**, 051801 (2011).

[13] A. Kalev, J. Shang, and B.-G. Englert, Phys. Rev. A **85**, 052116 (2012).

[14] R. Kosut, I. A. Walmsley, and H. Rabitz, arXiv: quant-ph/0411093.

[15] J. Nunn, B. J. Smith, G. Puentes, I. A. Walmsley, and J. S. Lundeen, Phys. Rev. A **81**, 042109 (2010).

[16] R. B. A. Adamson, L. K. Shalm, M. W. Mitchell, and A. M. Steinberg, Phys. Rev. Lett. **98**, 043601 (2007).

[17] R. B. A. Adamson, P. S. Turner, M. W. Mitchell, and A. M. Steinberg, Phys. Rev. A **78**, 033832 (2008).

[18] M. Asorey, P. Facchi, G. Florio, V. Man'ko, G. Marmo, S. Pascazio, and E. Sudarshan, Phys. Lett. A **375**, 861 (2011).

[19] A. M. Brańczyk, D. H. Mahler, L. A. Rozema, A. Darabi, A. M. Steinberg, and D. F. V. James, New J. Phys. **14**, 085003 (2012).

[20] D. Mogilevtsev, J. Řeháček, and Z. Hradil, New J. Phys. **14**, 095001 (2012).

[21] Y. S. Teo, B. Stoklasa, B.-G. Englert, J. Řeháček, and Z. Hradil, Phys. Rev. A **85**, 042317 (2012).

[22] S. T. Merkel, J. M. Gambetta, J. A. Smolin, S. Poletto, A. D. Córcoles, B. R. Johnson, C. A. Ryan, and M. Steffen, arXiv:1211.0322.

[23] J. B. Altepeter, E. R. Jeffrey, P. G. Kwiat, S. Tanzilli, N. Gisin, and A. Acín, Phys. Rev. Lett. **95**, 033601 (2005).

[24] J. Řeháček, Z. Hradil, E. Knill, and A. I. Lvovsky, Phys. Rev. A **75**, 042108 (2007).

[25] R. B. A. Adamson and A. M. Steinberg, Phys. Rev. Lett. **105**, 030406 (2010).

[26] Y. I. Bogdanov, G. Brida, M. Genovese, S. P. Kulik, E. V. Moreva, and A. P. Shurupov, Phys. Rev. Lett. **105**, 010404 (2010).

[27] K. Yamagata, Int. J. Quantum. Inform. **9**, 1167 (2011).

[28] G. Brida, I. P. Degiovanni, A. Florio, M. Genovese, P. Giorda, A. Meda, M. G. A. Paris, and A. P. Shurupov, Phys. Rev. A **83**, 052301 (2011).

[29] Y. I. Bogdanov, G. Brida, I. D. Bukeev, M. Genovese, K. S. Kravtsov, S. P. Kulik, E. V. Moreva, A. A. Soloviev, and A. P. Shurupov, Phys. Rev. A **84**, 042108 (2011).

[30] A. Kalev, J. Shang, and B.-G. Englert, Phys. Rev. A **85**, 052115 (2012).

[31] C. Flueraru, S. Latoui, J. Besse, and P. Legendre, IEEE Transactions on Instrumentation and Measurement **57**, 731 (2008).

[32] W. Wasilewski, P. Wasylczyk, P. Kolenderski, K. Banaszek, and C. Radzewicz, Opt. Lett. **31**, 1130 (2006).

[33] Z. Hradil, Phys. Rev. A **55**, R1561 (1997).

[34] M. S. Kaznady and D. F. V. James, Phys. Rev. A **79**, 022109 (2009).

[35] R. Blume-Kohout, New J. Phys. **12**, 043034 (2010).

[36] D. Gross, Y.-K. Liu, S. T. Flammia, S. Becker, and J. Eisert, Phys. Rev. Lett. **105**, 150401 (2010).

[37] Y. S. Teo, H. Zhu, B.-G. Englert, J. Řeháček, and Z. Hradil, Phys. Rev. Lett. **107**, 020404 (2011).

[38] R. Blume-Kohout, Phys. Rev. Lett. **105**, 200504 (2010).

[39] H. K. Ng and B.-G. Englert, arXiv:1202.5136.

[40] M. Christandl and R. Renner, Phys. Rev. Lett. **109**, 120403 (2012).

[41] R. Blume-Kohout, arXiv:1202.5270.

[42] D. S. Sabatke, M. R. Descour, E. L. Dereniak, W. C. Sweatt, S. A. Kemme, and G. S. Phipps, Opt. Lett. **25**, 802 (2000).